

# Investigation of structural, optical, magnetic properties and antibacterial activity of Ni-doped zinc oxide nanoparticles

S. B. Rana<sup>1</sup> · R. P. P. Singh<sup>2</sup>

Received: 28 February 2016 / Accepted: 9 May 2016 / Published online: 14 May 2016  
© Springer Science+Business Media New York 2016

**Abstract** In this study, pure ZnO and Ni doped ZnO nanoparticles were successfully synthesized by using the wet chemical precipitation method. Pure and Ni doped ZnO nanoparticles samples were characterized by X-ray diffraction (XRD), scanning electron microscopy (SEM), X-ray energy dispersive spectroscopy (EDS), UV–visible (UV–Vis) and FTIR spectroscopy. The XRD investigation of pure and Ni-doped ZnO nanoparticles samples reveal and confirm the formation of single phase hexagonal wurtzite structure, without formation of any secondary and other impurity phases. XRD results further reveals the shifting of characteristics peak toward higher  $2\theta$  (theta) angle with Ni doping. This shifting of the XRD peaks toward higher angle clearly indicates that Ni ions are effectively incorporated in the ZnO lattice. Surface morphology of pure and Ni doped ZnO nanoparticles samples was performed by using the SEM confirms the formation of spherical nanocrystallites with fine and clear defined boundaries. EDS spectroscopy indicates the substitution of dopant  $\text{Ni}^{2+}$  effectively in lattice site of  $\text{Zn}^{2+}$  as evident from XRD result also. The carriers i.e. donors confined on the Ni sites were confirmed from the micro Raman spectroscopy. Optical property of Ni-doped samples is confirmed by using the UV–Vis absorption which showed blue shift in absorption edge as compared to undoped ZnO nanoparticles. Undoped and Ni-doped ZnO nanoparticles

exhibit considerable changes in the M–H loop, specifically the diamagnetic response changed into ferromagnetic character for Ni doped samples in VSM investigation. The antibacterial activities of the Nickel doped zinc oxide were studied against Gram-negative (*Shigella dysenteriae*, *Vibrio cholerae*, and *E. coli*) via using agar well diffusion technique. Further, these Ni doped nanoparticles were then applied as antibacterial agent to control the microorganisms or bacterial growth. Ni-doping on zinc oxide and exposure of sunlight enhanced the antibacterial activity against bacterial pathogens which isolate at 40–45  $\mu\text{g}$  concentration. Interestingly in this study, most effective antibacterial results were obtained against the water related bacteria such as *E. coli* and *V. cholerae* for Ni-doped ZnO NPs.

## 1 Introduction

Compound semiconductor nanocrystals have interested different researchers because of their unusual and remarkable properties [1, 2]. In this category, Zinc oxide nanoparticles (ZnO) have been studied extensively from last few decades due to their potential exceptional applications in the field of optoelectronics due to its wide band-gap ( $\sim 3.37$  eV) and high exciton binding energy (60 meV) [3–5]. Recently, scientists and researchers are investigating the effect of doping ZnO nanoparticles with the transition metals such as Co, Fe and Mn. [6–10, 29]. Different theories have revealed that on doping ZnO nanoparticles with these transition elements results remarkable change in their different luminescent and magnetic properties. Further, the transition metal doped Zinc oxide semiconductors with room temperature ferromagnetism (RTFM) have been investigated for its

✉ S. B. Rana  
shashi\_rana12@yahoo.co.in

<sup>1</sup> Department of Electronics and Communication Engineering, Guru Nanak Dev University, Regional Campus, Gurdaspur, Punjab, India

<sup>2</sup> Department of Electronics and Communication Engineering, Arni University, Indora, H.P., India

advanced applications in the field of spintronics, where the effort was made to find the means and ways for effective utilization of these nanoparticles in both data storage and information processing [10–13]. In recent investigations, dilute magnetic semiconductor (DMSs) are formed by making the substitution of the cations on the host semiconductors material with small trace (doping) of the transition metal (TM) ions [14]. Transition metal doped semiconductors have attracted a lot of attention due to their significant applications such as short wavelength lasers, UV detectors, field-effect transistors, non linear varistors and high sensitive chemical sensors. These transition metals doping in semiconductor ZnO nanoparticles facilitates the generation of carrier induced ferromagnetism. In order to understand the underline mechanism in all these processes, it is absolutely essential to synthesize the ZnO based ferromagnetic material, where their physical and structural properties must be well understood explicitly. Experimental studies confirmed and revealed that the ferromagnetism (FM) strongly depends on synthesis methods and environmental conditions used for the synthesis of the samples. Numerous researchers addressed room temperature ferromagnetic behavior of transition metals (such as Co, Mn, Fe and Cr) doped zinc oxide nanoparticles [15–17]. Among all these magnetic-metals, nickel is one of the key dopant to achieve Curie temperature ( $T_c$ ) above the room temperature. Some researchers observed the paramagnetic and ferromagnetic nature in ZnO at RT with different composition of Ni content. Since the dilute magnetic semiconductor (DMS) contain a fraction of transition elements, thermal stability of the doped metal ions, which decide the material physical properties, are very essential for practical applications.

Several chemical methods have been developed to synthesize the nanoparticles (NPs) of various materials of interest. However, various chemical methods were used to prepare the ZnO based DMS materials, such as sol–gel method, hydrothermal, solvo-thermal, spray pyrolysis, co-precipitation method etc. [18–23]. The sol–gel technique is extensively used for the synthesis of novel ceramics material and for the preparation of crystalline material ores for metallurgical treatment. Among all these techniques, wet co-precipitation method has been extensively adopted to synthesis ZnO nanoparticles due to its economical (low) cost rate, offers larger degree of solubility of dopants and due to large yield of ZnO nanoparticles involved in the process [24–26].

Apart from this, Zinc oxide nanoparticles find many potential applications in various chemical and biological fields, including antibacterial agent and in bio labeling. ZnO NPS have revealed and shown good bacterial growth inhibiting character. The antibacterial activity of a material mainly depends on the production or generation of reactive

oxygen species (ROS) on the surface of the nanoparticles in the presence of light which further causes oxidative stress in bacterial cells. This phenomenon ultimately results in the death of the cells or micro-organisms [27–32]. Satumal et al. [33] suggested and reported that decrease in ZnO nanoparticles size with the increased presence of TM doping element (Ag and Ni) can be attributed to better solubility of dopant element on the surface of the nanoparticles. Thus, addition of Nickel in ZnO nanoparticles may result in varied particles size and hence may affect its antibacterial activity.

Prime focus of this study is just to ensure how these Ni-doped ZnO nanoparticles can be recommended as a probable water decontamination agent to protect water against the bacterial pathogens. So, Ni-doped ZnO nanoparticles were considered in this research paper to explore their effectiveness as a prospective candidate for biological applications, mainly as an antibacterial agent.

In this paper, the effect of Ni doping on the structural, morphological, elemental, optical and magnetic properties on ZnO nanoparticles were investigated by using XRD, SEM, EDS, UV–Vis and VSM study respectively. It was evident that by incorporating the Ni doping of ZnO nanoparticles not only results in increase in ferromagnetic properties in host semiconductor material but changes the lattice constant values in structural studies and changes the optical properties as well. These investigations were then followed by study of antibacterial activity of doped ZnO nanoparticles against harmful bacteria pathogens.

Organization related to this research paper is summarized as follows: Sect. 2, illustrate and explain the experimental procedure followed to synthesize the doped and pure (undoped) ZnO nanoparticles, followed by experimental procedure to measure the antibacterial activity of pure and Ni-doped ZnO. Thereafter, necessary instrumentation used to characterize the structural, optical, FTIR and magnetic properties of undoped and doped ZnO sample was highlighted. In Sect. 3, different results have been discussed in detail related to above mentioned properties, whereas the Sect. 4 concludes the paper.

## 2 Experimental method

### 2.1 Synthesis of pure and Ni-doped ZnO nanoparticles

All chemicals used in research work were procured from Sigma-Aldrich with purity level of 99.99 % and used without any other purification. In order to synthesize pure ZnO nanoparticles, zinc acetate hydrated [ $\text{Zn}(\text{CH}_3\text{COO})_2 \cdot 2\text{H}_2\text{O}$ ] (500 mg, 2, 0 mmol) was dissolved in distilled water and stirred for 1 h. Next, a sodium hydroxide

(NaOH) solution was added slowly in a drop-wise fashion to the mixture solution to maintain the pH  $\sim$  10. The solution mixture was then stirred at room temperature for about 3 h followed by aging for 24 h at the identical temperature. After this step, white precipitates that formed were then centrifuged, filtered and washed several times (distilled water) and were finally annealed at 500 °C for 2 h. In order to synthesize Ni-doped ZnO nanocrystals, nickel acetate [Ni (CH<sub>3</sub>COO)<sub>2</sub>·2H<sub>2</sub>O] was mixed with Zinc Acetate solution in accordance with the calculated stoichiometric ratio. The required quantity of aqueous NaOH solution was then added drop by drop to the mixture solution to get (pH  $\sim$  10). The method for the precipitation of undoped ZnO nanoparticles was followed for the synthesis of Ni doped ZnO NPs.

## 2.2 Determination of antimicrobial activity

Antimicrobial activities of the synthesized pure ZnO and Ni doped ZnO NPs were performed against three pathogens namely Gram-negative (*Shigella dysenteriae*, *Salmonella typhi* and *E. coli*). The antibacterial activity of pure ZnO and Ni-doped ZnO was performed by using nanoparticles diffusion method [34]. Particular cultures of microorganisms were created on nutrient broth at 35 °C by shaking the incubator at 200 rpm. Each and every isolated bacterial culture was homogeneously spread on the plates with the help of sterile spreader. Bacterial culture lawn on nutrient agar plate was arranged by spreading the 150  $\mu$ l liquid culture. Agar plates were kept in the standing position for about 20 min, so that the culture gets absorbed. The 9 mm size wells were then inserted into the agar by the use of head sterile micropipette tips. Each well is then sealed from the bottom by 10  $\mu$ l of molten agar in order to avoid the leakage of loaded sample onto the surface of petri plate. After this step, nanomaterial's (doped ZnO) suspension in the distilled water (60  $\mu$ g/100  $\mu$ l) was poured into each well of plate. Under the controlled incubation condition for about 35 degree centigrade for the 24 h it results in formation of zone of inhibition in form of bacterial growth retardation which were then subsequently measured. In this set up, distilled water was used to provide the blank control and tetracycline is used as a positive control. After this another set of nanomaterial loaded well plate was prepared and exposed for 2 h in sunlight under the incubated optimum temperature.

## 2.3 Characterization of pure and Ni-doped ZnO samples

To accurately investigate the structural properties of undoped and Ni-doped ZnO nanoparticles XRD was performed by using the X-ray diffractometer (model no.

Bruker AXS D8, Germany) which is equipped with graphite monochromator and a mirror fixed at the incidence angle of 1°–5°. In this set up, we were using CuK $\alpha$  (Wavelength = 1.540 Å, 40 kV, 100 mA) as the radiation source. The angular accuracy of this setup was fixed at 0.001° and the angular resolution was kept about 0.01°. The samples were scanned in angular direction which varies from 20° to 90° (2-theta) with step size of 0.01°. Surface morphology or structural properties of pure and doped synthesized samples was ascertained and estimated by using scanning electron microscope Carl Zeiss Supras 55 which operates at a high accelerated voltage of 15 kV. In order to investigate the optical properties of samples, the UV absorption spectra of these samples were recorded on the double beam spectrophotometer (Systronics-2205) having bandwidth of 1 nm and wavelength ranges from 300 to 800 nm. Elemental composition of various sample were ascertained by using EDS spectroscopy at an acceleration voltage of 200 keV. Raman spectroscopic investigation was performed by the using imaging spectrograph which consists of 400 mm focal length laser Raman spectrometer (SEKI). The presence of various functional groups was ascertained by using Fourier transform infra red (FTIR) spectroscopy using Thermo Nicolet 390 with KBr pellet technique at room temperature in the range 400–4000 cm<sup>-1</sup>. Magnetic hysteresis (M–H) loop at room temperature (RT) was measured by using the Vibrating Sample Magnetometer (VSM, Microsense EZ8) having maximum magnetic field strength of 22.6 kOe.

## 3 Results and discussions

In this study, one of our aims was to highlight the various results obtained by using different investigation techniques for Ni-doped ZnO nanoparticles, but for comparison sake we included the results obtained for undoped ZnO nanoparticles. This has enabled us to compare the various structural, optical, magnetic and antibacterial activities of undoped and Ni-doped ZnO nanoparticles.

### 3.1 XRD analysis of undoped and Ni-doped ZnO nanoparticles

In this study, we compared the synthesized undoped ZnO nanoparticles crystallite size with that of Ni doped ZnO by using XRD technique. Figure 1a, b shows X-ray diffraction (XRD) patterns of the synthesized undoped (pure ZnO) and Nickel doped (Zn<sub>0.95</sub>Ni<sub>0.05</sub>O) samples. Each XRD sample exhibit the hexagonal wurtzite phase without any impurities and secondary phase formation.

It is clearly from XRD pattern (spectra) that all the characteristic diffraction peaks can be indexed to the

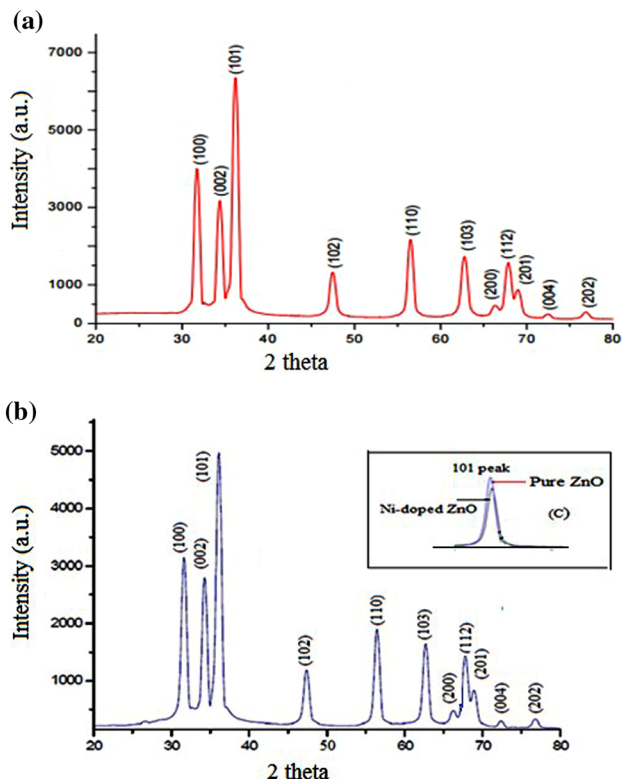


**Fig. 1** XRD spectra of **a** pure and **b** Ni-doped ZnO nanoparticles, **c** shifting of (101) peak toward higher angle for Ni-doped ZnO NPs

diffractions of (100), (002), (101), (102), (110), (103), (200), (112), (201), (004) and (202) planes with the clear hexagonal wurtzite structure [35]. These diffraction peaks are in close agreement with the standard value of JCPDS card no. 01-079-2206 card. From the XRD pattern of Fig. 1a, b it is clear that the Ni-doped samples shows lowering of intensity peak as compared to undoped (pure) ZnO NPs. This lowering of intensity of diffraction peaks of Ni-doped sample signifies that the crystalline character of the ZnO NPs had reduced considerably due to Ni doping. Further, we observe that the characteristic peak of (101) plane related to doped sample shift toward the higher angle as compared to undoped (pure) ZnO NPs as shown in Fig. 1c and illustrated in the subsequent discussion. Apart from this phenomenon, we also observe the broadening of XRD peak of Ni-doped samples reveals that size of doped ZnO nanoparticles is smaller than the undoped ZnO NPs. The decrease in the crystallite size is chiefly due to the distortion in a host ZnO lattice by the introduction of impurities and the presence of Ni<sup>2+</sup> reduces the nucleation and consequent growth rate of ZnO NPs. Close examination of the XRD spectra further revealed that some XRD peaks appearing in undoped ZnO NPs at higher angles disappear in the Ni doped ZnO samples. This is due to the reduction of grain size and presence of strain in the ZnO lattice due to

introduction of Ni dopant atom in host ZnO matrix. Hence, we conclude that small change in 2-theta values of diffraction peaks and broadening of peak are due to the increase in micro-strain and the line broadening effect is mainly caused by the size and micro-strain of doped ZnO nanoparticles. Doped ZnO NPs size reduction is significant as compared to undoped NPs and highlighted in Table 1.

Figure 1c clearly shows the shifting of characteristics peak toward higher 2θ (theta) angle value with Ni doping. This shifting of the peak positions clearly indicates that Ni ions are completely diffused (incorporated) in the Zn position in the ZnO lattice [36].

However, the average crystallite size can be deduced and calculated by using Scherrer’s Eq. (1) and was calculated to be in the range of 41–45 nm for doped to undoped ZnO NPs and highlighted in Table 1.

$$\tau = \frac{k\lambda}{\beta \cos\theta} \tag{1}$$

In above equation, τ is grain size, β is the full width at half maxima, λ is the wavelength of X-ray used (1.547 Å) and θ is the angle of diffraction. Table 1 clearly showed that lattice strain and dislocation density increases with the doping of Ni ion as compared with undoped NPs as highlighted in Table 1. From the d spacing values, lattice constant ‘a’ and ‘c’ can be calculated by using the Eq. (2) and their values are shown in Table 1.

$$\frac{1}{d^2} = \frac{4}{3} \left( \frac{h^2 + hk + k^2}{a^2} \right) + \frac{1}{c^2} \tag{2}$$

The ionic radius value for doped element Ni<sup>2+</sup> is 69 pm and for Zn<sup>2+</sup> its value is 74 pm. It is clearly observed from the Table 1 that value of lattice parameters and d value goes on reducing due to the smaller ionic radius of Ni ions due the substitution of Zn<sup>2+</sup> by Ni<sup>2+</sup> during the doping process.

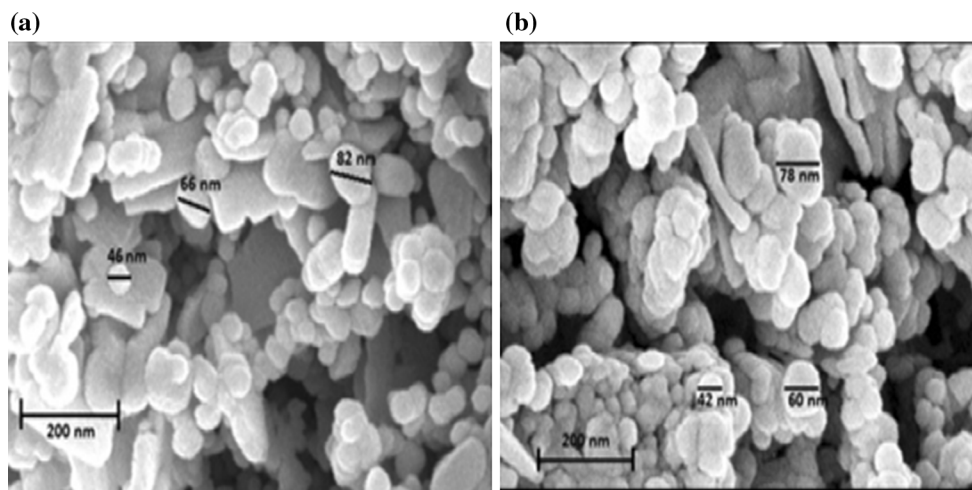
### 3.2 Scanning electron microscope (SEM) analysis

The surface morphology of pure and Ni-doped samples was carried by using the scanning electron microscopy (SEM) investigation. Figure 2a, b shows the SEM images of pure and Zn<sub>0.95</sub>Ni<sub>0.05</sub>O nanoparticles samples with an average particle size of around 65 and 60 nm respectively. The SEM micrograph of pure ZnO nanoparticles sample revealed that these nano particles are spherical in shape with large aggregation. It is clearly evident from the Fig. 2b that aggregation is almost restricted in Ni-doped ZnO NPs sample, and particles appears in uniform and consistent shape with slightly constricted size distribution. The nanoparticle size calculated from XRD spectra is relatively different from the SEM micrograph measurement



**Table 1** Nanostructural properties of pure ZnO and Ni-doped ZnO nanoparticles

Sample	Particle size (nm)	Lattice strain	Dislocation density $\times 10^{-14}$ line <sup>2</sup> /m <sup>2</sup>	$d_{101}$ (Å)	Lattice constant	
					a	c
Pure ZnO	45	0.0027	4.92	2.4767	3.234	5.281
Ni-doped ZnO	41	0.0030	5.67	2.4754	3.233	5.279

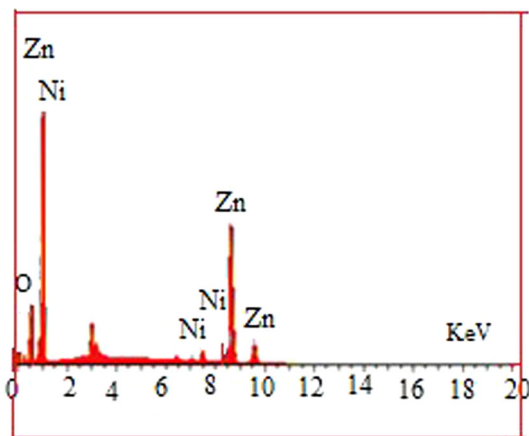
**Fig. 2** SEM images of **a** pure ZnO, **b** Ni doped ZnO nanoparticles

because in SEM, computation related to size of particles are performed by taking the difference of clear (noticeable) grain boundaries, but the XRD measurements are taken from the crystalline surface area which diffracts the X-ray waves reasonably or effectively [37].

From Fig. 2b, it is clear that doped nanoparticles size goes on decreasing because dopant  $\text{Ni}^{2+}$  is diffusing evenly or homogeneously in the different sites and are noticeably visible with less porosity in the background environment (portion). Hence, it is clear from SEM micrograph that pure ZnO NPs appears in bigger form, while doped ( $\text{Zn}_{0.95}\text{Ni}_{0.05}\text{O}$ ) nanoparticles appears in smaller size which verifies our XRD results.

Elemental composition of the synthesized ZnO nanoparticles (doped and undoped) was determined from the energy dispersive X-ray spectroscopy (EDS) as shown in Fig. 3. The EDS analysis confirms the presence of Ni, O and Zn in the doped sample with no presence of any other impurity element or phase. Figure 3 shows the EDS spectra of Ni-doped ZnO NPs sample.

The EDS spectrum indicates that the synthesized Ni-doped ZnO sample mainly contain Zn, Ni and O elements. The EDS spectral peaks of O appeared at 0.5 keV, Zn appeared at 1, 8.5 and 9.6 keV respectively. Result of EDS spectra further confirm and verify the XRD result, which

**Fig. 3** EDS spectra of Ni doped ZnO nanoparticles

reveals that Ni doped ZnO NPs were successful synthesized by the wet chemical precipitation method.

### 3.3 Optical absorption study

Optical properties of undoped ZnO NPs become increasingly more and more prominent when size of particle is reduced in nanoscale. Optical properties of pure ZnO and Ni-doped ZnO NPs were successfully investigated by

employing UV–visible absorption spectroscopy. The band gap of these compound semiconductor nanoparticles varies as the different dopants can cause (create) different crystal defect in the ZnO crystal structure. The UV–visible absorption investigation of pure ZnO and Ni-doped ZnO nanoparticles is shown in Fig. 4 in the wavelength ranges from 300 to 800 nm. Absorbance value is exclusively dependent on the various factors like size of nanoparticles and deformities or defects in grain structure. The UV–Vis spectrum of undoped ZnO NPs shows the edge absorption peak at 390 nm due to exciton recombination at room temperature [38]. As the Ni doping concentration is changed from pure ZnO the absorption edge is start to shift towards lower wavelengths (blue shift) which further imply that the band gap ( $E_g$ ) increases, which will be due to strain or defects. All these factors leads to the reduction of crystallite size of Ni doped ZnO sample, which further verifies our result of XRD spectra. Figure 4, shows the absorption spectra of the pure ZnO and Ni doped ZnO nanoparticles with the absorption peak at 390, 387 nm respectively.

Table 2, summarizes the band gap energy ( $E_g = hc/\lambda$ ) value for undoped (pure) and Ni-doped ZnO nanoparticles. The optical band gap value calculated in our pure ZnO sample is small (3.19 eV) as compared with standard band gap value of bulk ZnO material i.e. 3.3 eV. But, the observed  $E_g$  value is in good agreement with the  $E_g$  value highlighted in literature [39]. The increase in band gap energy with the increase of Ni content is attributed to the incorporation of  $Ni^{2+}$  ions into the ZnO host lattice.

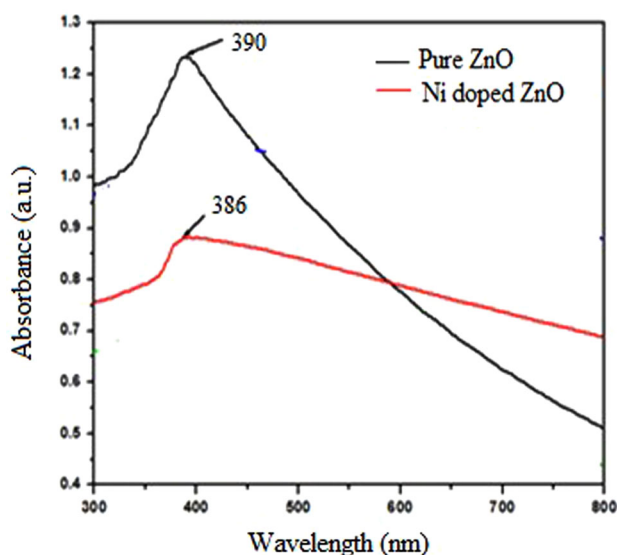


**Fig. 4** UV–visible absorption spectra of Pure ZnO and Ni doped ZnO nanoparticles

This phenomenon of increase in band gap energy ( $E_g$ ) and absorption at the lesser wavelength can also be explained on the basis of quantum confinement effect amongst the individual doped ZnO nanoparticles.

### 3.4 FTIR study of pure (undoped) and Ni doped ZnO nanoparticles

An FTIR spectrum was used to give the information about the chemisorbed species, elemental constituent of material and presence of various functional groups in the material. It also gives the information related to presence of outgoing and incoming species that may exist on the surface of material. Various series of the peak ranges from 400 to  $4000\text{ cm}^{-1}$  are found to be present in FTIR spectra, which show the existence of various functional groups and chemisorbed species in undoped and doped ZnO. Apart from this, FTIR spectroscopic investigation revealed the vibrational frequencies of undoped (pure) ZnO and doped ZnO nanoparticles. The FTIR spectra for pure and doped ZnO NPs are shown in Fig. 5.

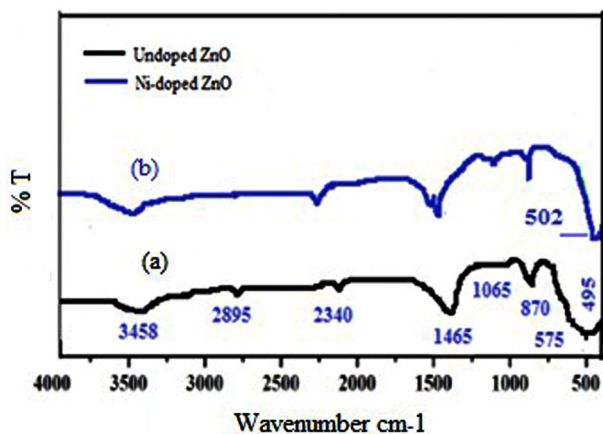
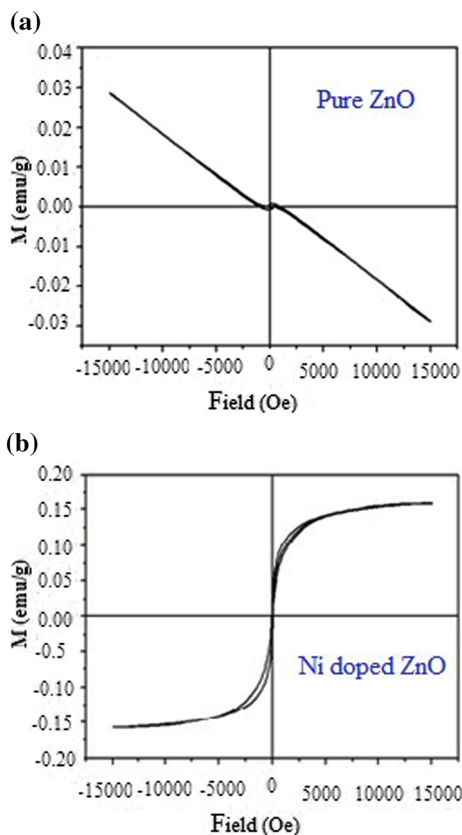
The presence of absorption peak between  $3025$  and  $3655\text{ cm}^{-1}$  corresponds to the vibration mode of O–H group [40]. The absorption peaks observed at the value of  $3458\text{ cm}^{-1}$  are due to the presence of O–H stretching of surface adsorbed  $H_2O$  molecules in Ni-doped and undoped sample. The peaks found at  $2855$  and  $2955\text{ cm}^{-1}$  are due to the symmetric and asymmetric nature of C–H group. The absorption peak found at  $2340\text{ cm}^{-1}$  was due to the existence of  $CO_2$  molecules in the air [22]. Presence of the weak absorption band found around  $870\text{ cm}^{-1}$  was due to the Ni–O vibrational frequency due to the presence of Nickel in the ZnO lattice structure [41]. In case of undoped ZnO, the absorption band of Zn–O stretching was found at  $577\text{ cm}^{-1}$ . Presence of peak at  $502\text{ cm}^{-1}$  for Ni doped ZnO nanoparticles will be attributed due to the inclusion of  $Ni^{2+}$  in ZnO host matrix. This peak was found to be absent in FTIR spectra of pure ZnO NPs. The minor change found in the observed values will be due to stretching of Zn–O–Ni bond. When ZnO NPs samples are calcined above  $500\text{ }^\circ\text{C}$ , various functional groups are removed from ZnO nanoparticles surface easily. Observations related to FTIR spectroscopy are found to be in good agreement with XRD results as discussed earlier.

### 3.5 VSM study of pure and doped ZnO nanoparticles

Magnetization measurements related to pure and Ni-doped ZnO nanoparticles were carried out by using the vibrating sample magnetometer (VSM) which uses the magnetic hysteresis (M–H) curve. In this set up all the measurements were carried out at the room temperature. Synthesized pure

**Table 2** Band gap energy ( $E_g$ ) variation of pure ZnO versus Ni-doped ZnO nanoparticles

Sample	Absorption wavelength ( $\lambda$ ) (nm)	Band gap energy ( $E_g = hc/\lambda$ ) (eV)
Pure ZnO	390	3.19
Ni doped ZnO	386	3.23

**Fig. 5** FTIR spectra of (a) undoped ZnO and (b) Ni-doped ZnO nanoparticles**Fig. 6** M–H curve of a pure ZnO, b Ni-doped ZnO nanoparticles at room temperature

ZnO NPs sample clearly shows the diamagnetic behavior (property) as shown in Fig. 5a. Diamagnetic behavior (nature) of pure ZnO NPs has been reported in literature [42].

From the magnetic hysteresis loops or M–H curve of Fig. 6b it is clear that the Ni-doped sample show the ferromagnetic behavior at room temperature (RT). Table 3, shows the value of magnetization saturation ( $M_s$ ) and remanent ( $M_r$ ) in case of Ni-doped ZnO sample due to ferromagnetic nature of Ni-doped sample. Various assumptions associated with exhibition of room temperature ferromagnetism behavior have been addressed i.e. secondary phase, clusters and ferromagnetism due to various defects in our following discussion.

So far, different theories have been proposed regarding the origin of ferromagnetism this subject is still controversial. One of hypothesis proposed that room temperature (RT) ferromagnetism of Ni-doped samples is exhibited due to different intrinsic and extrinsic phenomenon. Intrinsic phenomenon's normally occurs due exchange interaction and extrinsic phenomenon occurs due to formation of secondary phases and nanoclusters or secondary phases of dopant (Ni) semiconductor atoms [43]. The linkage between intrinsic defects such as Zinc or oxygen vacancies and associated magnetism is also discussed in various research papers. However, in our investigation, the XRD and EDS spectra results clearly showed that dopant ions (Ni) are effectively incorporated in the Zinc (Zn) wurtzite lattice structure without formation of any metallic clusters or secondary phases. Consequently, probability of ferromagnetism exhibition due to formation of secondary phases and metallic clusters is entirely ruled out in case of Ni-doped sample.

Among other mechanism accountable for ferromagnetism, the oxygen mediated exchange interaction among the dopant ions (Ni) could be the probable mechanism responsible for the observed ferromagnetic nature of the Ni-doped samples. Das et al. [44], proposed that exchange interaction mechanism mediated by the oxygen vacancies (Ni–O–Ni) is mainly responsible for increase in magnetic saturation when the dopant Ni is doped on the ZnO NPs, as

**Table 3** Magnetization response measurement

Sample	$H_C$ (Oe)	$M_r$ (emu/g)	$M_s$ (emu/g)
Ni doped ZnO NPs	75	0.0026	0.023

process of doping increases carriers concentration in the form of oxygen vacancies. Increase in the value of saturation magnetization value at room temperature, is the best possible mechanism for exhibition of room temperature ferromagnetism of Ni-doped sample.

From the analysis of XRD, EDS and VSM of our samples, it is sensible to say that observed room temperature (RT) ferromagnetism is an intrinsic property of doped material sample and not result due to formation of any metallic clusters or secondary phases.

### 3.6 Raman spectroscopy of pure and doped ZnO nanoparticles

Raman spectroscopy is considered as one of most versatile method for detecting the incorporation of dopant and lattice defects in the host lattice structure [4, 45]. The surface of doped nanoparticles gets modified due to charge transport between the dopant and host material, which results in change of optical Raman spectrum [46].

Figure 7 shows the Raman spectra of the doped and undoped ZnO NPs at room temperature in the range 100–700  $\text{cm}^{-1}$ . In case of undoped ZnO NPs, the strong and intense peak appearing at 435  $\text{cm}^{-1}$  has been designated as high frequency branch for the E2 mode of ZnO NPs. The different peaks appearing at 162, 333 and 575  $\text{cm}^{-1}$  has been chosen as second-order vibration mode [2E2], the optical mode (transverse) with A1 symmetry [A1] and the optical phonon mode (longitudinal) with E1 symmetry [E1] respectively [47]. The blue shift in Raman spectra is observed and the corresponding peak value is 540  $\text{cm}^{-1}$  for Ni-doped ZnO NPs samples. The Raman spectra of Ni-doped ZnO shows the presence of large vibration mode centered around 532–540  $\text{cm}^{-1}$  which can be chosen (assigned) as local

vibrational mode associated with the Ni doping, which are bounded with the various donor defects. These various donor defects can be Zinc interstitials and doubly oxygen vacancies defects which are the characteristic shallow donor defects in ZnO NPs.

### 3.7 Antibacterial activity of pure and doped ZnO nanoparticles

In the present study, pure and Ni doped ZnO nanoparticles were tested against three pathogens namely; *S. dysenteriae*, *V. cholerae* and *E. coli* using the nanoparticles diffusion technique. Different researchers have proposed that the antibacterial effectiveness of ZnO nanoparticles are generally depends on the presence of reactive oxygen species (ROS), which is mostly resulted due to the larger surface area of NPs, release of  $\text{Zn}^{2+}$  and increase in oxygen vacancies. The hydroxyl radical, superoxide and hydrogen peroxide related to the ROS group can cause appreciable harm to DNA and may lead to death of cell [48]. In general, nanoparticles with improved photocatalytic activity have smaller crystalline size and large surface, which increases oxygen vacancies and resulting more reactive oxygen species ROS. The presence of more number of reactive oxygen species (ROS) is mainly resulted due to two main factors (a) diffusion capability of the different reactants (b) the formation of more and more oxygen vacancies. The antibacterial activity of the ZnO nanoparticles is mainly due to the oxygen vacancies which further depend on presence of  $\text{Zn}^{2+}$  ions [49]. The increase of Nickel doping in ZnO nanoparticles can produce more number of defects which were further verified and confirmed by XRD results. Due to nickel doping the dislocation density and strain (which represent the defects) are found to be increased as observed in XRD results.

Antibacterial activity of Ni-doped ZnO NPs can be illustrated by using optical source of 600 nm wavelength. By illuminating the sample with 600 nm light, the defects in doped sample generate electron–hole pairs. The holes split the water molecule ( $\text{H}_2\text{O}$ ) into ( $\text{OH}^-$  and  $\text{H}^+$ ) molecules from the ZnO NP's suspension. Dissolved oxygen molecules present in solution are changed into the superoxide anions ( $\text{O}_2^-$ ), which sequentially react with  $\text{H}^+$  to produce ( $\text{HO}_2$ ) radicals, which upon consequent collision with electrons that result in production of hydrogen peroxide anions ( $\text{H}_2\text{O}_2^{2-}$ ). This hydrogen peroxide anion ( $\text{H}_2\text{O}_2^{2-}$ ) then reacts with hydrogen ions to produce the molecules of  $\text{H}_2\text{O}_2$ . The generated molecule of  $\text{H}_2\text{O}_2$  can infiltrate the cell membrane and kills the microorganism or bacteria [50]. However, during the reaction the excess ROS is produced, which can cause numerous sub cellular physical

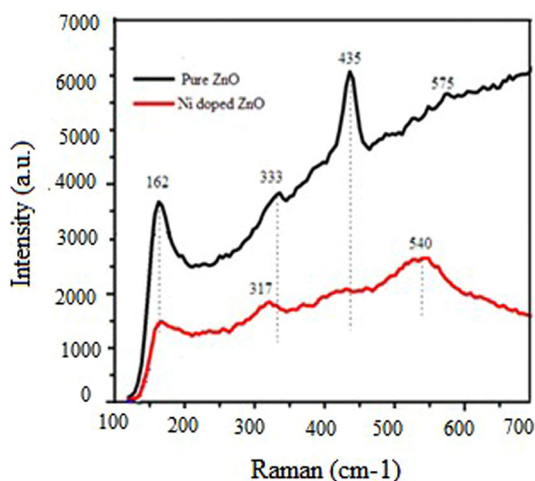


**Fig. 7** Raman spectra of pure and doped ZnO nanoparticles



damage such as membrane, DNA damage and protein denaturation. In this work, the Nickel doped ZnO NPs exhibit enhanced antibacterial activity than the undoped ZnO NPs.

In our study, antimicrobial activity of pure ZnO nanoparticles was highest against *E. coli* ( $17 \pm 0.4$ ) and lowest against *S. dysenteriae* ( $12 \pm 0.5$ ) as highlighted in Table 4.

However, for Ni-doped zinc oxide nanoparticles, antibacterial activity was enhanced significantly (30, 25 and 23 %) against *S. dysenteriae*, *V. cholerae* and *E. coli*, respectively. However, photo-catalytically exposure (2 h) of ZnO nanomaterials showed enhancement of (22, 25, 29 and 27 %) activity against *S. dysenteriae*, *S. typhi*, *V. cholerae* and *E. coli*, respectively. For undoped (pure) ZnO nanoparticles growth inhibition rate was found to be increased by exposure of sun light as compared to unexposed plate by 16, 7 and 5 % for *S. dysenteriae*, *V. cholerae* and *E. coli*, respectively as highlighted in Table 4. Furthermore, we compared the antibacterial growth pattern for *S. dysenteriae*, *V. cholerae* and *E. coli* growth patterns in the Ni-doped and undoped ZnO nanoparticles under the exposure of sunlight (2 h). Growth of bacteria in the sample (100  $\mu\text{g/ml}$ ) of pure and Ni-doped zinc oxide nanoparticles were recorded in nutrient broth medium for (a) *S. dysenteriae* (b) *V. cholerae* (c) *E. coli* depicted in (Fig. 8).

Zhang et al. [51] have previously reported the ZnO bactericidal property in *E. coli*, *S. typhi*, *B. subtilis* and *S. aureus*. The unusual bactericidal behavior of ZnO and Ni-doped ZnO might be due to chemical interactions between nanomaterials and membrane proteins and formation of free radicals in the presence of ZnO nanoparticles.

In nutshell, aim of this study is to investigate how synthesized Ni-doped ZnO nanoparticles can be used as an effective and strong antibacterial agent against three water borne bacteria in presence and absence of sunlight. These research finding encourage us to use Ni-doped ZnO nanoparticles as a potential antibacterial agent in various biological and pharmaceutical applications in future.

**Table 4** Zone of inhibition for bacterial growth in pure and doped ZnO nanoparticles without and with the exposure of sunlight

Treatment	Diameter zone of inhibition (mm)		
	<i>S. dysenteriae</i>	<i>V. cholerae</i>	<i>E. coli</i>
Without sunlight exposure			
Pure ZnO	$12 \pm 0.5$	$16 \pm 0.5$	$17 \pm 0.4$
Ni-doped ZnO	$17 \pm 1.2$	$21 \pm 1.2$	$23 \pm 1.5$
Exposure with sunlight (2 h)			
Pure ZnO	$16 \pm 0.5$	$19 \pm 0.5$	$20 \pm 0.4$
Ni-doped ZnO	$19 \pm 1.2$	$24 \pm 1.2$	$25 \pm 1.5$

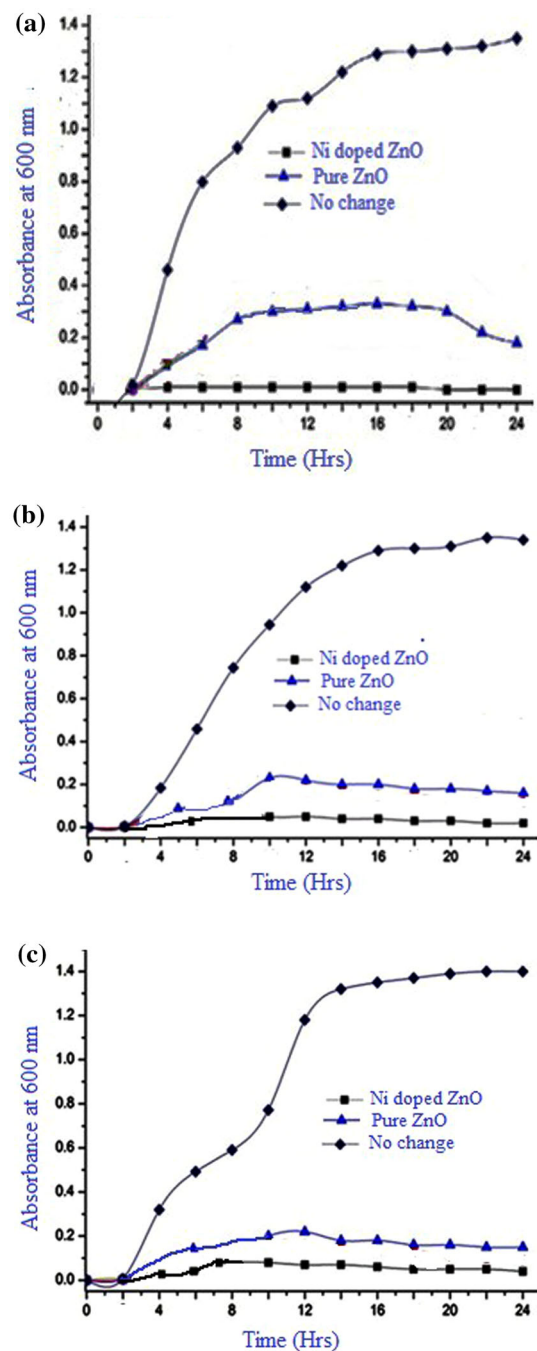


**Fig. 8** Growth response or pattern of bacteria in pure and Ni-doped ZnO nanoparticles for three pathogens a *S. dysenteriae*, b *V. cholerae*, c *E. coli*

## 4 Conclusions

In this research investigation, wet chemical synthesis of pure and nickel-doped ZnO nanoparticles were successfully achieved with clear wurtzite structure. XRD spectra confirmed the incorporation of  $\text{Ni}^{2+}$  ions into the lattice site of  $\text{Zn}^{2+}$  ions in the host ZnO matrix. Spherical morphology of pure and doped ZnO nanoparticles was

confirmed by using the SEM technique. EDS spectroscopy confirmed the elemental composition of Zn, O and Ni proved the presence of nickel ions as dopant ion in host lattice. UV-absorption spectrum shows blue shift in wavelength for nickel doped sample as compared with pure ZnO nanoparticles sample. Increase in band gap proved the successful incorporation of Ni<sup>2+</sup> ions in ZnO matrix. From VSM studies of pure and doped ZnO nanoparticles, it is observed that pure ZnO shows diamagnetic nature whereas Ni doped samples exhibit ferromagnetic property at room temperature. Due to soft (dilute) magnetization offered by Ni-doped ZnO NPs, we can use this material as potential candidate for spintronics application. The antibacterial studies performed against three pathogens shows that the Ni-doped ZnO possessed a better antibacterial effect than undoped or pure ZnO nanoparticles.

## References

- D. Shuang, X.X. Zhu, J.B. Wang, X.L. Zhong, G.J. Huang, C. He, *Appl. Surf. Sci.* **257**, 6085 (2011)
- J. Das, D.K. Mishra, D.R. Sahu, S.K. Pradhan, B.K. Roul, *J. Magn. Magn. Mater.* **323**, 641 (2011)
- V. Ischenko, S. Polarz, D. Grote, V. Stavarache, K. Fink, M. Driess, *Adv. Funct. Mater.* **15**, 1945 (2003)
- S.S. Kurbanov, G.N. Panin, T.W. Kim, T.W. Kang, *Phys. Rev. B* **78**, 045311 (2008)
- W. Zhang, J. Zhao, Z. Liu, Z. Liu, *Appl. Surf. Sci.* **284**, 49 (2013)
- D. Karmakar, S.K. Mandal, R.M. Kadam, P.L. Paulose, A.K. Rajarajan, T.K. Nath, A.K. Das, I. Dasgupta, G.P. Das, *Phys. Rev.* **B75**, 144404 (2007)
- S. Chattopadhyaya, T.K. Nath, A.J. Behan, J.R. Neal, D. Score, Q. Feng, A.M. Fox, G.A. Gehring, *Appl. Surf. Sci.* **257**, 381 (2010)
- J.M.D. Coey, M. Venkatesan, C.B. Fitzgerald, *Nat. Mater.* **4**, 173 (2005)
- F. Pan, C. Song, X.J. Liu, Y.C. Yang, F. Zeng, *Mater. Sci. Eng. R Rep.* **62**, 1 (2008)
- J.M.D. Coey, *J. Appl. Phys.* **97**, 10D313 (2005)
- L.B. Duan, G.H. Rao, Y.C. Wang, J. Yu, T. Wang, *J. Appl. Phys.* **104**, 013909 (2008)
- H.W. Zhang, Z.R. Wei, Z.Q. Li, G.Y. Dong, *Mater. Lett.* **61**, 3605 (2007)
- N.N. Lathiotakis, A.N. Andriotis, M. Menon, *Phys. Rev. B* **78**, 193311 (2008)
- X. Du, Y. Fu, J. Sun, X. Han, J. Liu, *Semicond. Sci. Technol.* **21**, 1202 (2006)
- M. Chakrabarti, S. Dechoudhury, D. Sanyal, T.K. Roy, D. Bhowmick, A. Chakrabarti, *J. Phys. D* **41**, 135006 (2008)
- H.S. Hsu, J.C.A. Huang, Y.H. Huang, T.F. Liao, M.Z. Lin, C.H. Lee, J.F. Lee, S.F. Chen, L.Y. Lai, C.O. Liu, *Appl. Phys. Lett.* **88**, 242507 (2006)
- K. Potzger, S. Zhou, H. Reuther, A. Mucklich, F. Eichhorn, N. Schell, W. Skorupa, M. Helm, J. Fassbender, T. Herrmannsdorfer, T.P. Papageorgiou, *Appl. Phys. Lett.* **88**, 052508 (2006)
- S.B. Rana, A. Singh, N. Kaur, *J. Mater. Sci. Mater. Electron.* **24**, 44 (2013)
- Y.Q. Wang, S.L. Yuan, L. Liu, P. Li, X.X. Lan, Z.M. Tian, J.H. He, S.Y. Yin, *J. Magn. Magn. Mater.* **320**, 1423 (2008)
- S. Kaviya, J. Santhanalakshmi, B. Viswanathan, J. Muthumary, K. Srinivasan, *Spectrochim. Acta, Part A* **79**, 594 (2011)
- R. Brayner, R. Ferrari-Iliou, N. Brivois, S. Djediat, M.F. Benedetti, F. Fievet, *Nano Lett.* **6**, 866 (2006)
- G.X. Tong, F.F. Du, Y. Liang, Q. Hu, R.N. Wu, J.G. Guan, X. Hu, *J. Mater. Chem. B* **1**, 454 (2013)
- Z. Liu, Q. Zhang, G. Shi, Y. Li, H. Wang, *J. Magn. Magn. Mater.* **323**, 1022 (2011)
- M. Salavati-Niasari, A. Khansari, F. Davar, *Inorg. Chim. Acta* **362**, 4937 (2009)
- P. Ball, L. Garwin, *Nature* **355**, 761–766 (1992)
- S.B. Rana, P. Singh, A.K. Sharma, R. Dogra, *J. Optoelectron. Adv. Mater.* **12**, 257 (2010)
- M.G. Pei, C. Xia, B. Wu, T. Wang, L. Zhang, Y. Dong, J. Xu, *Comput. Mater. Sci.* **43**, 489 (2008)
- J.C. Johnson, H. Yan, P. Yang, R.J. Saykally, *J. Phys. Chem. B* **107**, 8816–8828 (2003)
- Z. Fan, J.G. Lu, *Appl. Phys. Lett.* **86**, 123510 (2005)
- P.V. Radovanovic, D.R. Gamelin, *Phys. Rev. Lett.* **91**, 157202 (2003)
- H.T. Ng, J. Han, T. Yamada, P. Nguyen, Y.P. Chen, M. Meyyappan, *Nano Lett.* **7**, 1247 (2004)
- R.Y. Hong, J.Z. Qian, J.X. Cao, *Powder Technol.* **163**, 160 (2006)
- B. Staumal, B. Baretjky, A. Mazilkin, S. Protasiba, A. Petrastrumal, *J. Eur. Ceram. Soc.* **29**, 1963 (2009)
- K. Ueda, H. Tabata, T. Kawai, *Appl. Phys. Lett.* **79**, 988 (2001)
- C. Xai, C. Hu, Y. Tian, B. Wan, J. Xu, X. He, *Phys. E* **42**, 2086 (2010)
- Z. Zhang, E.-W. Shi, Z.-Z. Chen, *Mater. Sci. Semicond. Process.* **13**, 132 (2010)
- S. Maensiri, C.P. Laokul, V. Promarak, *J. Cryst. Growth* **289**, 102 (2006)
- G. Vijayaprasath, G. Ravi, A.S.H. Hameed, T. Mahalingam, *J. Phys. Chem. C* **118**, 9715 (2014)
- M. Arshad, A. Azama, A.S. Ahmed, S. Mollah, A.H. Naqvi, *J. Alloys Compd.* **509**, 8378 (2011)
- H. Liu, J. Yang, Z. Hua, Y. Zhang, L. Yang, L. Xiao, Z. Xie, *Appl. Surf. Sci.* **256**, 4162 (2010)
- P. Gopal, N.A. Spaldin, *Phys. Rev. B* **74**, 094418 (2006)
- R. Saravanan, K. Santhi, N. Sivakumar, V. Narayanan, A. Stephen, *Mater. Charact.* **67**, 10 (2012)
- Y. Liu, T. Wang, X. Sun, Q. Fang, Q. Lv, X. Song, Z. Sun, *Appl. Surf. Sci.* **257**, 6540 (2011)
- J. Das, D.K. Mishra, D.R. Sahu, B.K. Roul, *Mater. Lett.* **65**(4), 598 (2011)
- J. Cui, U. Gibson, *Phys. Rev. B* **74**, 045416 (2006)
- H.D. Li, S.F. Yu, A.P. Abiyasa, Y. Clement, S.P. Lau, H.Y. Yang, E.S.P. Leong, *Appl. Phys. Lett.* **86**, 261111 (2005)
- L.W. Yang, X.L. Wu, G.S. Huang, T. Qiu, Y.M. Yang, *J. Appl. Phys.* **97**, 014308 (2005)
- J. Becker, K.R. Raghupathi, J.S. Pierre, D. Zhao, R.T. Koodali, *J. Phys. Chem. C* **115**, 13844 (2011)
- E.V. Skorb, L.I. Antonouskaya, N.A. Belyasova, D.G. Shchukin, H. Möhwald, D.V. Sviridov, *Appl. Catal. B* **84**, 94 (2008)
- A.S.H. Hameed, C. Karthikeyan, S. Sasikumar, V.S. Kumar, S. Kumaresan, G. Ravi, *J. Mater. Chem. B* **1**, 5950 (2013)
- L. Zhang, Y. Jiang, Y. Ding, N. Daskalakis, L. Jeuken, M. Povey, A.J. O'Neill, D.W. York, *J. Nanopart. Res.* **12**, 1625 (2010)